



# Synthesis, characterization and semiconducting behavior of N,2,5-trisubstituted pyrroles

Olivia Monroy<sup>a</sup>, Lioudmila Fomina<sup>a</sup>, María Elena Sánchez-Vergara<sup>b</sup>, Rubén Gaviño<sup>c</sup>, Alonso Acosta<sup>a</sup>, José Ramón Álvarez Bada<sup>b</sup>, Roberto Salcedo<sup>a,\*</sup>

<sup>a</sup> Instituto de Investigaciones en Materiales, Universidad Nacional Autónoma de México, Circuito Exterior s/n, Ciudad Universitaria, Coyoacán, 04510, Ciudad de México, Mexico

<sup>b</sup> Universidad Anáhuac México, Campus Norte, Avenida Universidad Anáhuac 46, Col. Lomas Anáhuac, Huixquilucan, 52786, Estado de México, Mexico

<sup>c</sup> Instituto de Química, Universidad Nacional Autónoma de México, Circuito Exterior s/n, Ciudad Universitaria, Coyoacán, 04510, Ciudad de México, Mexico

## ARTICLE INFO

### Article history:

Received 6 February 2018

Accepted 28 May 2018

Available online 29 May 2018

### Keywords:

Diphenyl-pyrrole derivatives

Semiconductor monomers

DFT calculations

Optical band gap

## ABSTRACT

In this work, N,2,5-trisubstituted pyrroles were synthesized and characterized by IR, UV–Vis and NMR spectroscopies. These materials' electronic and optical properties were then evaluated. Theoretical calculations were carried out by means of the Gaussian09 software and all the involved species were geometrically optimized in order to obtain the theoretic HOMO, LUMO and band gaps. From the HOMO and LUMO calculations, it turns out that monomer 1-(3,5-dinitrophenyl)-2,5-diphenyl-1H-pyrrole could be used as a *p*-type semiconductor or *n*-type semiconductor, depending on the substituent. The experimental optical band gaps were obtained by the Tauc and Cody methods and compared to the ones calculated through DFT. The results show that the semiconducting behavior is found in all the monomers and depends on the functional group of the structure, its crystallinity degree, as well as its HOMO and its LUMO energies.

© 2018 Elsevier B.V. All rights reserved.

## 1. Introduction

In the last decades, the study of organic semiconductors has been of great importance due to their potential applications in electronic devices, such as organic light-emitting diodes (OLEDs) [1], field-effect transistors [2], sensors [3] and solar cells [4]. The distinctive feature of organic semiconductors, in contrast to inorganic semiconductors, is their solid-state structure, which is based on weak interactions, mainly Van der Waals and dipole-dipole interactions among nearest neighbors, resulting in a wide range of conductive behaviors, from insulators to conductors [5]. This type of materials also presents other special properties, such as flexibility for chemical synthesis, ease to modify their structures and simple processing, that make them attractive for several applications. This functionality depends mainly on the interaction between HOMO (High Occupied Molecular Orbital) and LUMO (Low Unoccupied Molecular Orbital) energy levels [6], the energetic difference between LUMO and HOMO being known as band gap [7].

A band gap characteristic of semiconductor materials permits low-energy excitations, meaning that the material has the capability to easily donate an electron (from the HOMO), or receive it (in the LUMO), which is the elementary process occurring in every organic electronic device. In commercial devices, the desirable band gaps for optimal efficiency are in the 1.59–3.18 eV range [8] within the wider semiconductor range of 1–4 eV [9]. There are different methods to determine the band gap in organic materials. *Ab initio* density functional (DFT) calculations can be used to estimate the HOMO and LUMO energy levels for the band gap determination [10], while the Tauc and Cody methods can be used to determine the optical band gap [11,12]. The Tauc method [11,13] is frequently used to derive the band gap in terms of the incident energy. The Tauc band gap associated with semiconductor materials is determined through an extrapolation of the linear trend observed in the spectral dependence of  $(\alpha h\nu)^n$  over a limited range of photon energies  $h\nu$  [11,14]. The Cody model assumes that this behavior is due to a fundamental curvature in the spectral dependence of  $(\alpha h\nu)^n = f(h\nu)$ , which is held responsible for increases in the Tauc optical gap related to decreasing thickness [12,14]. In accordance to this model, as defined by the Cody method, the band gap associated with semiconductors should be determined by extrapolating the linear

\* Corresponding author.

E-mail address: [salcevitch@gmail.com](mailto:salcevitch@gmail.com) (R. Salcedo).

trend observed in the spectral dependence of  $(\alpha/h\nu)^n$  versus  $h\nu$ .

Among the semiconductor materials under study, those that contain substituted heterocycles in their structure, such as pyrrole, stand out [15]. Substituted pyrrole is well known for its different applications in drug chemistry [16], organic electronics [17] and photoluminescence materials [18]. Trisubstituted pyrroles have also been subject of interest [19–23]. Materials of this type can be monomers or polymers with electron-withdrawing groups, but all the materials under consideration in this work are monomers. These monomers have the structure shown in Diagram 1, where the substituents are –O-Me, –OH, –CN, –COOH and –NO<sub>2</sub> and are located in the *para* position of the aromatic ring joined to the nitrogen atom from pyrrole. In all cases, the capability of the substituents for withdrawing electron density is well-known, resulting in two main effects: (i) promoting an inductive effect and (ii) tuning HOMO and LUMO energy levels. Therefore, these materials show a decrease in the band gap energy, obtaining smaller values than those for the unsubstituted monomer (4.451 eV). However, in the case of –NO<sub>2</sub> substituents, these effects are stronger than the ones shown by other compounds of this family. This feature leads to a dipolar behavior and an electronic current through a route directed towards the electron-withdrawing substituent. The narrowest band gap has a value of 3.02 eV; consequently, this material has a semiconducting behavior. The electronic structure and properties of this type of materials depend on the degree of conjugation along the molecular skeleton. Interest in monomers has been growing due to their versatility, since their properties can be modified by changing from amorphous to crystalline structure. High hole mobility (of up to 0.1 cm<sup>2</sup>/V) occurs in ordered monomer structures, unlike polymers, in which polydispersity linked to the synthesis occurs. The mixture of compounds that make up the polymer does not usually show the same composition and, thus, the reproducibility of its optoelectronic properties cannot be fully guaranteed. Moreover, the high probability of finding defects in the conjugated polymer chains and their low crystallinity make charge mobility in the polymers lower than that in the monomers.

The purpose of this work is to report the synthesis and characterization of monomers prepared from 1,4-diphenyl-1,3-butadiene and aromatic amines with one or two different electron-withdrawing substituents in order to study the source of the semiconducting behavior of the materials and propose new materials with interesting electronic behavior. The theoretical band gap of these monomers was estimated from DFT calculations and compared with the values obtained from Cody and Tauc semi-empirical methods, based on spectroscopic measurements. Band gap determination also provides fundamental information regarding the electronic properties of semiconductors. For instance, the band gap controls the nature of the electroluminescent signals in OLEDs and, in photovoltaic cells, it determines light absorption efficiency.

## 2. Experimental

All chemicals were provided by Aldrich Chemical Company and used as received. The FT-IR spectra data were collected with a Thermo Scientific, Nicolet 6700 spectrophotometer with an ATR Smart Orbit attachment. <sup>1</sup>H and <sup>13</sup>C NMR spectra for all compounds were registered with Bruker, Avance 300 MHz and Bruker, Avance III HD 400 MHz spectrometers. The chemical shifts are reported in ppm, scaled relative to TMS. All melting points were registered on a Fischer-Jones melting-point apparatus and are uncorrected.

*Synthesis of the precursor compound.* 1, 4-diphenylbuta-1,3-diene [24–26]. To a solution of phenyl acetylene (2.042 g, 20 mmol) in iso-propanol was added CuCl (I) (0.4 g, 4 mmol) and N, N, N', N'-tetramethylethylenediamine (TMEDA), 0.1 ml (0.077 g, 0.6 mmol).

The mixture was stirred for 3 h under a stream of oxygen, and the subsequent solution added to acidified water. The product was separated by filtration, dried in vacuum and purified by recrystallization from hexane. Yield: 95%, white solid, m.p. 86 °C. FT-IR:  $\nu(\text{C}\equiv\text{C}) = 2148 \text{ cm}^{-1}$ ,  $\nu(\text{C-H}) = 3050 \text{ cm}^{-1}$ . <sup>1</sup>H NMR (300 MHz, CDCl<sub>3</sub>):  $\delta$  7.34 (m, 3H), 7.53 (m, 2H). <sup>13</sup>C NMR (75 MHz, CDCl<sub>3</sub>):  $\delta$  73.92, 81.55, 121.81, 128.43, 129.19, 132.49.

*Synthesis of monomers (1–8).* The monomers were synthesized using the procedure reported previously by some authors [19,21,23]. A mixture of precursor (0.50 g, 2.47 mmol), CuCl (I) (0.04 g, 0.49 mmol) and the appropriate amine (4.94 mmol), in DMF (10 ml), was refluxed under a nitrogen atmosphere for 48 h at 153 °C in an oil bath, then allowed to cool at room temperature. The solvent was removed in vacuum and the product was purified by column chromatography using hexane or a hexane-acetone mixture as eluent.

- (1) 1-(3,5-dinitrophenyl)-2,5-diphenyl-1H-pyrrole. Yield: 50%, orange solid, m.p.: 216 °C. FT-IR:  $\nu(\text{C-N}) = 1382 \text{ cm}^{-1}$ ,  $\nu(\text{C=C}) = 1448, 1463, 1483, 1599 \text{ cm}^{-1}$ ,  $\nu_{\text{as}}(\text{NO}_2) = 1537 \text{ cm}^{-1}$ ,  $\nu_{\text{s}}(\text{NO}_2) = 1335 \text{ cm}^{-1}$ ,  $\delta(\text{NO}_2) = 847 \text{ cm}^{-1}$ . <sup>1</sup>H NMR (400 MHz, CDCl<sub>3</sub>):  $\delta$  6.55 (s, 2H, H-pyrrole), 7.09 (m, 4H), 7.27 (m, 6H), 8.08 (d, 2H), 8.86 (t, 1H). <sup>13</sup>C NMR (100 MHz, CDCl<sub>3</sub>):  $\delta$  110.98 (C-pyrrole), 111.78, 116.59, 127.68, 128.44, 128.62, 129.33, 131.74, 135.88, 147.98.
- (2) 1-(4-nitro-3-(trifluoromethyl)phenyl)-2,5-diphenyl-1H-pyrrole. Yield: 80%, yellow solid, m.p.: 185 °C. FT-IR:  $\nu(\text{C-N}) = 1365 \text{ cm}^{-1}$ ,  $\nu(\text{C=C}) = 1417, 1449, 1488, 1598 \text{ cm}^{-1}$ ,  $\nu_{\text{as}}(\text{NO}_2) = 1535 \text{ cm}^{-1}$ ,  $\nu_{\text{s}}(\text{NO}_2) = 1301 \text{ cm}^{-1}$ ,  $\delta(\text{NO}_2) = 852 \text{ cm}^{-1}$ ,  $\nu(\text{CF}_3) = 1245 \text{ cm}^{-1}$ . <sup>1</sup>H NMR (400 MHz, CDCl<sub>3</sub>):  $\delta$  6.51 (s, 2H, H-pyrrole), 7.04 (m, 6H), 7.13 (m, 1H), 7.26 (m, 5H), 7.75 (d, 1H). <sup>13</sup>C NMR (100 MHz, CDCl<sub>3</sub>):  $\delta$  111.70 (C-pyrrole), 124.09, 125.75, 127.39, 127.85, 128.47, 128.65, 129.18, 130.65, 132.11, 135.61, 142.56, 145.40.
- (3) 1-(2-nitro-4-(trifluoromethyl)phenyl)-2,5-diphenyl-1H-pyrrole. Yield: 50%, white solid, m.p.: 79 °C. FT-IR:  $\nu(\text{C-N}) = 1360 \text{ cm}^{-1}$ ,  $\nu(\text{C=C}) = 1461, 1603 \text{ cm}^{-1}$ ,  $\nu_{\text{as}}(\text{NO}_2) = 1510 \text{ cm}^{-1}$ ,  $\nu_{\text{s}}(\text{NO}_2) = 1376 \text{ cm}^{-1}$ ,  $\delta(\text{NO}_2) = 842 \text{ cm}^{-1}$ ,  $\nu(\text{CF}_3) = 1243 \text{ cm}^{-1}$ . <sup>1</sup>H NMR (400 MHz, CDCl<sub>3</sub>):  $\delta$  6.78 (s, 2H, H-pyrrole), 7.32 (t, 3H), 7.45 (t, 5H), 7.80 (d, 5H). <sup>13</sup>C NMR (100 MHz, CDCl<sub>3</sub>):  $\delta$  107.25 (C-pyrrole), 123.74, 127.36, 128.73, 130.80, 153.37.
- (4) 1-(2,4-dinitrophenyl)-2,5-diphenyl-1H-pyrrole. Yield: 40%, white solid, m.p.: 56 °C. FT-IR:  $\nu(\text{C-N}) = 1379 \text{ cm}^{-1}$ ,  $\nu(\text{C=C}) = 1441, 1489, 1570, 1596 \text{ cm}^{-1}$ ,  $\nu_{\text{as}}(\text{NO}_2) = 1539 \text{ cm}^{-1}$ ,  $\nu_{\text{s}}(\text{NO}_2) = 1382 \text{ cm}^{-1}$ ,  $\delta(\text{NO}_2) = 848 \text{ cm}^{-1}$ . <sup>1</sup>H NMR (300 MHz, CDCl<sub>3</sub>):  $\delta$  6.73 (s, 2H, H-pyrrole), 7.27 (m, 3H), 7.39 (m, 5H), 7.75 (m, 5H). <sup>13</sup>C NMR (75 MHz, CDCl<sub>3</sub>):  $\delta$  107.20 (C-pyrrole), 123.71, 127.33, 128.69, 128.80, 130.77, 153.35.
- (5) 1-(4-nitro-2-(trifluoromethyl)phenyl)-2,5-diphenyl-1H-pyrrole. Yield: 50%, white solid, m.p.: 80 °C. FT-IR:  $\nu(\text{C-N}) = 1363 \text{ cm}^{-1}$ ,  $\nu(\text{C=C}) = 1439, 1484, 1568, 1592 \text{ cm}^{-1}$ ,  $\nu_{\text{as}}(\text{NO}_2) = 1529 \text{ cm}^{-1}$ ,  $\nu_{\text{s}}(\text{NO}_2) = 1385 \text{ cm}^{-1}$ ,  $\delta(\text{NO}_2) = 849 \text{ cm}^{-1}$ ,  $\nu(\text{CF}_3) = 1285 \text{ cm}^{-1}$ . <sup>1</sup>H NMR (400 MHz, CDCl<sub>3</sub>):  $\delta$  6.78 (s, 2H, H-pyrrole), 7.31 (m, 3H), 7.45 (t, 5H), 7.79 (m, 5H). <sup>13</sup>C NMR (100 MHz, CDCl<sub>3</sub>):  $\delta$  107.24 (C-pyrrole), 123.73, 127.36, 128.72, 130.80, 153.37.
- (6) 1-(4-fluoro-3-(trifluoromethyl)phenyl)-2,5-diphenyl-1H-pyrrole. Yield: 80%, white solid, m.p.: 211 °C. FT-IR:  $\nu(\text{C-N}) = 1319 \text{ cm}^{-1}$ ,  $\nu(\text{C=C}) = 1433, 1482, 1504, 1600 \text{ cm}^{-1}$ ,  $\nu(\text{CF}_3) = 1321 \text{ cm}^{-1}$ ,  $\nu(\text{C-F}) = 1120 \text{ cm}^{-1}$ . <sup>1</sup>H NMR (400 MHz, CDCl<sub>3</sub>):  $\delta$  6.48 (s, 2H, H-pyrrole), 7.04 (m, 5H), 7.16 (m, 1H), 7.21 (m, 7H). <sup>13</sup>C NMR (100 MHz, CDCl<sub>3</sub>):  $\delta$  110.48 (C-pyrrole), 117.18, 117.39, 126.83, 127.41, 128.14, 128.94, 132.57, 133.85, 133.94, 135.11, 135.87.

- (7) 2,5-diphenyl-1-(4-(trifluoromethyl)phenyl)-1H-pyrrole. Yield: 90%, white solid, m.p.: 209 °C. FT-IR:  $\nu(\text{C}=\text{C}) = 1463, 1485, 1520, 1600 \text{ cm}^{-1}$ ,  $\nu(\text{CF}_3) = 1332 \text{ cm}^{-1}$ .  $^1\text{H}$  NMR (300 MHz,  $\text{CDCl}_3$ ):  $\delta$  6.49 (s, 1H, H-pyrrole), 7.03 (m, 2H), 7.10 (d, 1H), 7.19 (m, 3H), 7.48 (d, 1H, H-9).  $^{13}\text{C}$  NMR (75 MHz,  $\text{CDCl}_3$ ):  $\delta$  110.68 (C-pyrrole), 122.03, 125.75, 125.79, 125.84, 125.89, 126.64, 128.10, 128.88, 129.06, 132.81, 135.77, 142.01.
- (8) 1-(4-fluorophenyl)-2,5-diphenyl-1H-pyrrole. Yield: 70%, white solid, m.p.: 256 °C. FT-IR:  $\nu(\text{C}-\text{N}) = 1287 \text{ cm}^{-1}$ ,  $\nu(\text{C}=\text{C}) = 1398 \text{ cm}^{-1}$ ,  $\nu(\text{C}-\text{F}) = 1229 \text{ cm}^{-1}$ .  $^1\text{H}$  NMR (400 MHz,  $\text{CDCl}_3$ ):  $\delta$  6.50 (s, 1H, H-pyrrole), 6.96 (m, 1H), 7.02 (m, 1H), 7.09 (m, 2H), 7.21 (m, 3H).  $^{13}\text{C}$  NMR (100 MHz,  $\text{CDCl}_3$ ):  $\delta$  109.99 (C-pyrrole), 115.61, 115.83, 126.39, 127.98, 128.78, 130.33, 130.41, 133.05, 135.02, 135.89.

X-ray diffraction analysis was performed with the  $\theta$ -2 $\theta$  technique using a Bragg-Brentano geometry with a Bruker, D8 Avance diffractometer and working with  $\text{CuK}\alpha$  ( $\lambda = 0.15405 \text{ nm}$ ) radiation. For the optical properties, the UV–vis spectroscopy of the monomers was measured on a Unicam spectrophotometer, model UV300, in the wavelength range of 200–1100 nm. The Tauc and Cody band gap values of monomers were calculated from the absorption coefficient and photon energy. Additionally, the types of electronic transitions in the N, 2,5-trisubstituted pyrroles were obtained.

### 3. Theoretical

All calculations were carried out by means of the Gaussian09 code [27]. For the structures of all the derivatives, Becke's gradient corrections [28] for exchange and Perdew-Wang's parameterization for correlation [29] were applied. This is the scheme of the B3PW91 method. The calculations were performed using the 6-31G\*\* basis set. In all cases, frequency calculations were carried out in order to assess thermodynamic stability as well as the theoretical IR spectra, which were compared with the experimental ones.

### 4. Results and discussion

The diphenyl-pyrrole based monomer syntheses are shown in Diagram 2. The diyne compound precursor for that reaction was obtained through a modification of Hay's oxidative coupling, employing  $\text{CuCl}$  (I) as a catalyst [30].

The diacetylene thus obtained was then made to react with aromatic amines with electron-withdrawing substituents, according to the Reisch-Shulte procedure under nitrogen, using  $\text{CuCl}$  (I) at 153 °C during 48 h [19,24–26]. Polar solvents like DMF favor the formation of pyrroles. The conversion of the diacetylenic group was studied by FT-IR and NMR spectroscopy. The  $^1\text{H}$  spectra of the monomer compounds showed singlets at 6.47–6.74 ppm. In the  $^{13}\text{C}$  NMR spectrum, signals at 73.92 and 81.55 ppm disappear after reaction. The signals at 107.20–111.70 ppm in the  $^{13}\text{C}$  spectra are attributed to 2,5-disubstituted pyrrole. The monomers derived from ortho-substituted amines exhibit lower yields than those obtained from meta- and/or para-substituted amines, due to the steric hindrance.

As mentioned earlier, all the monomers in this study correspond to the general formula shown in Diagram 2. The differences in all of them arise from the nature and position of the substituents on the terminal aromatic ring. It is well known that the substituents have a very important effect when trying to obtain the desired properties. The substitution with electron withdrawing substituents produces lower energetic differences between the HOMO-LUMO frontier orbitals, higher electron affinities and higher ionization potentials. In contrast, electron donating substituents have an opposite effect

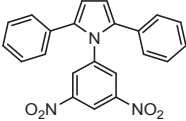
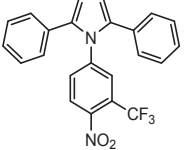
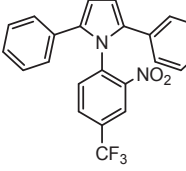
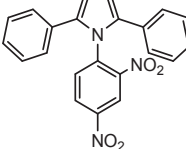
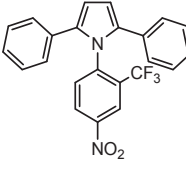
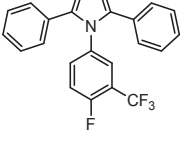
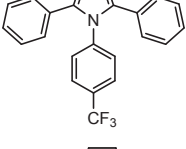
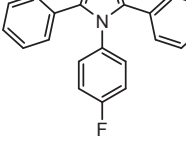
on HOMO and LUMO energy orbitals because of enlarged electron density in the structure [31,32]. Studies of monomers with only one electron withdrawing substituent in the *para* position have previously been reported [21], obtaining a narrow band gap between the frontier orbitals. In this work, the study has been extended to improve the semiconducting behavior by changing the nature of the substituent or introducing more substituents which are also electron withdrawing and may reinforce the phenomenon. The geometry of the general compound leads to an electronic flow which can run from the pyrrole to the aromatic ring or in the reverse direction, depending on the nature of the substituents. This study focuses on the influence of this effect on the global behavior of the resulting compounds. The results are presented in two separate sections, one about the theoretical calculations and another with the experimental data. A comparison and the corresponding discussion is made at the end.

#### a) Theoretical results

The theoretical calculations were carried out to explain the experimental data. The main features to consider are the frontier molecular orbitals behavior and the theoretical spectroscopy. Considering the data shown in Diagram 1, it is important to ascertain the semiconducting nature of the several compounds reported there. The main feature to consider is the presence in all the important cases of the  $-\text{NO}_2$  substituent; there are other important electron withdrawing groups, but it seems that the presence of this particular group yields the best results, therefore the discussion focus on this isolated case. The particular phenomenon in which the presence of the electron withdrawing groups are related to the semiconducting behavior has been previously studied and discussed [21]. Nevertheless, in this work it is important to highlight that the electronic effect is larger when the group is  $-\text{NO}_2$ , therefore the first compounds in Table 1 were chosen in such a way that this group be included, with several other electron withdrawing substituents for comparison.

Fig. 1 shows the HOMO-LUMO set for the molecules which bear this substituent. The case shown there corresponds to a dinitro case; however, the behavior is exactly the same for all molecules which have at least one nitro substituent. HOMO is localized on the pyrrole and its lateral aromatic rings moiety, whereas LUMO is completely localized on the aromatic ring joined to the nitrogen atom from the pyrrole and with a strong participation of the substituents. The HOMO and LUMO values calculated for different monomers are shown in Table 1. If monomers are to be used as organic semiconductors, it is necessary to separately consider the values of HOMO and LUMO energies. The *p*-type semiconductors, or hole conveyors, have low levels of HOMO energy, allowing easy hole injection and high hole mobility. On the contrary, *n*-type semiconductors will be those that have low LUMO energy levels and high electron mobility [33]. The HOMO values shown in Table 1 are very similar for all the monomers, suggesting that they follow the same trend regarding hole mobility. The lower value corresponds to monomer 1, which is an indication that this monomer could be used as *p*-type semiconductor. On the other hand, the monomer 8, with the  $-\text{F}$  group, seems to behave as *n*-type semiconductor. It is known that electron-attracting functional groups, such as  $-\text{F}$  or  $-\text{CF}_3$ , can promote electronic conduction [33]. This fits with the observation in Table 1 that monomer 7 is the second one with the highest HOMO after monomer 8. Apparently, the presence in the same molecule of two electron-attracting groups, as occurs in monomer 6, does not favor electronic conduction, since it has two active sites from which electrons can flow. Regarding LUMO, it can be observed in Table 1 that there are important differences among the studied monomers. As in the HOMO case, monomer 1 is the one

**Table 1**  
HOMO and LUMO values and comparison of experimental and theoretical band gap results of the synthesized compounds.

Compound	Structure	Name	Frontier Orbitals (eV)		Band gap (eV)		
			HOMO	LUMO	DFT	Tauc	Cody
1		1-(3,5-dinitrophenyl)-2,5-diphenyl-1H-pyrrole	-5.796	-3.700	2.096	2.1	2.1
2		1-(4-nitro-3-(trifluoromethyl)phenyl)-2,5-diphenyl-1H-pyrrole	-5.714	-3.374	2.340	2.2	2.1
3		1-(2-nitro-4-(trifluoromethyl)phenyl)-2,5-diphenyl-1H-pyrrole	-5.660	-3.238	2.422	2.5	2.6
4		1-(2,4-dinitrophenyl)-2,5-diphenyl-1H-pyrrole	-5.697	-3.238	2.449	2.8	2.7
5		1-(4-nitro-2-(trifluoromethyl)phenyl)-2,5-diphenyl-1H-pyrrole	-5.551	-2.802	2.749	2.7	2.9
6		1-(4-fluoro-3-(trifluoromethyl)phenyl)-2,5-diphenyl-1H-pyrrole	-5.523	-1.632	3.891	3.3	3.3
7		2,5-diphenyl-1-(4-(trifluoromethyl)phenyl)-1H-pyrrole	-5.442	-1.442	4.0	3.3	3.3
8		1-(4-fluorophenyl)-2,5-diphenyl-1H-pyrrole	-5.306	-0.761	4.545	2.7	2.4

with the significantly lowest LUMO value and would behave as *n*-type semiconductor, facilitating electron mobility. The HOMO and LUMO energy values obtained for monomer **1**, makes it a strong candidate for use in the manufacture of devices, such as OLEDs, because, upon substituent change, it can be used as both *p*-type semiconductor and *n*-type semiconductor.

Another important aspect of the semiconductor materials used in the manufacture of optoelectronic devices is a band gap that, in

monomers and polymers, generally varies between 1.5 y 4eV [9]. The theoretical model suggests that the inductive effect is fundamental to get a short band gap, the explanation being that the electronic flow caused by the aromatic cloud has a definitive direction which is defined by the delocalized negative charge between both oxygen atoms of the  $-\text{NO}_2$  group. Therefore, the HOMO (bearing to the majority aromatic system) which has the least electrons tends to approach towards the empty function of the

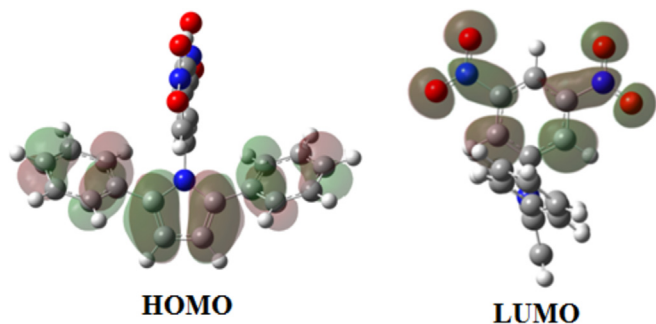


Fig. 1. Frontier molecular orbitals of molecules which contain  $-\text{NO}_2$ .

LUMO, shortening the gap. The trend is similar in other compounds with electron-withdrawal effect, but is stronger in this case. Fig. 2 shows the shape and location of frontier molecular orbitals corresponding to the structures which do not include  $-\text{NO}_2$  substituents. In these cases, the influence of the groups  $-\text{CF}_3$  and  $-\text{F}$  is generally evident. The DFT band gap in these substances is relatively larger than in the  $-\text{NO}_2$  cases, the explanation of this situation arising from the same MO analysis.

The HOMO in these cases shows exactly the same behavior as in their  $-\text{NO}_2$  counterparts, but the LUMO is predominantly localized on the aromatic ring joined to the nitrogen atom from the pyrrole ring, and this situation differs from the first case, in which the majority of the LUMO functions is on the  $-\text{NO}_2$  substituent. This suggests that the electronic flow is almost the same in all cases, i.e. the electrons flow from the lateral aromatic rings of the pyrrole to the substituted ring, but the strongest electronic flow is directed towards the  $-\text{NO}_2$  molecules. The DFT band gap shown in Table 1 suggests that monomer **8** has an insulating behavior, with a band gap higher than 4 eV. Nevertheless, the DFT band gap should first be compared to experimental values in order to clearly define its electrical properties.

Comparison of the theoretical and experimental data validates the calculations, Fig. 3a/b shows the experimental and theoretical spectra for the monomers **1**, **2**, **7**, **8**. The main peaks for the specific substituents are indicated, the comparison of all the cases shows that the structure of the new molecules is correct, the more relevant matching arises when the C-N stretching peaks of all cases are compared because they appear at the expected position (with slight variations since theoretical model does not take into account the environmental effect). These bands are located between 1280 and 1390  $\text{cm}^{-1}$ . In the case of monomer **8** the peak has low oscillator strength and appears at 1287 and 1310  $\text{cm}^{-1}$  for both the experiment and the calculations. It is important to note that this particular signal gains importance when the  $-\text{NO}_2$  substituent is present,

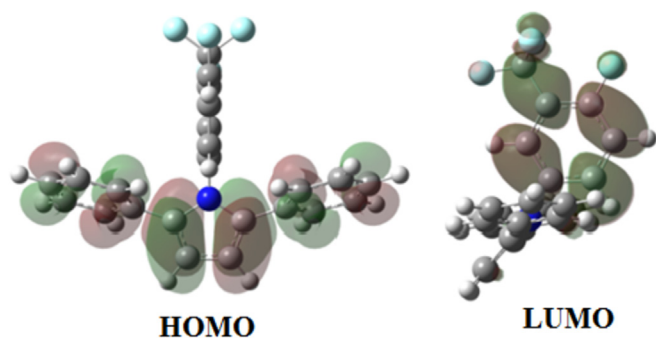


Fig. 2. HOMO-LUMO set of molecules without  $-\text{NO}_2$  substituent.

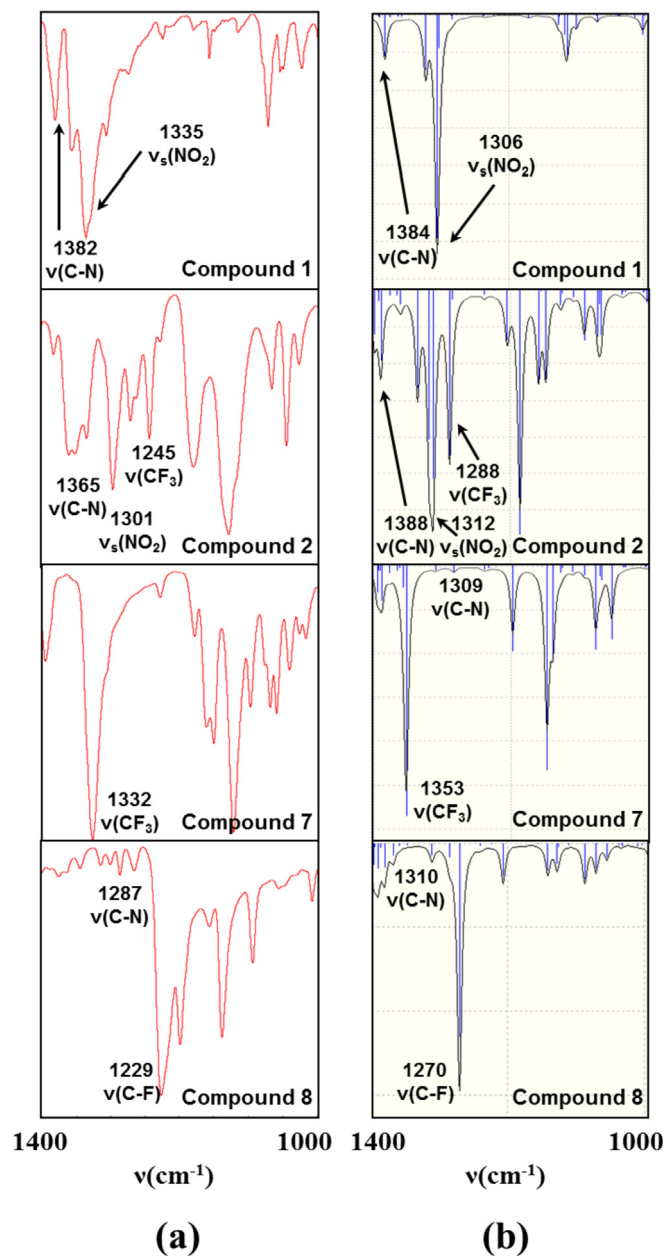


Fig. 3. (a) Experimental infrared spectra and (b) theoretical infrared spectra for the compounds **1**, **2**, **7**, **8**.

but this is not the case of monomer **8**. The case of monomer **7** is different because the corresponding peak of the C-N stretching does not appear because of the overlap with a strong band at 1332  $\text{cm}^{-1}$  originated from the stretching modes of the  $-\text{CF}_3$  substituent. Another important effect is a shift of the C-N stretching band when the  $-\text{NO}_2$  substituent is present, due to the strong inductive effect of this group. The cases of the monomers **1** and **2** which have the  $-\text{NO}_2$  group are easy to interpret, the symmetric stretch band is strong and appears between 1301 and 1335  $\text{cm}^{-1}$ , it seems that the difference in position arises from the fact that monomer **1** has two  $-\text{NO}_2$  groups. Monomer **2** has the  $-\text{NO}_2$  group as well as  $-\text{CF}_3$ , the last one appears at 1245  $\text{cm}^{-1}$  in the experimental spectrum whereas it is localized at 1288  $\text{cm}^{-1}$  in the theoretical one, this same signal appears in the spectrum of monomer **7** at 1332 and 1353  $\text{cm}^{-1}$  respectively. Another important band to note is the C-F stretching of the monomer **8**, this band is important

because the group C-F corresponds to the F atom directly linked to the aromatic ring, this frequency appears at  $1229\text{ cm}^{-1}$  for the experimental and  $1270\text{ cm}^{-1}$  for the theoretical spectra. Despite small differences arising from gas phase calculations, all cases show good agreement with experiment.

## b) Experimental results

Optical absorption measurements are widely used to characterize the electronic properties of monomers through the determination of parameters, such as the band gap, describing the electronic transitions [34]. The optical absorbance spectra of the monomers were recorded from 250 to 700 nm and are shown in Fig. 4a. The intermolecular band appearing in the high energy region between 280 and 380 nm refers to electronic transitions inside the monomer, because there is an electronic delocalization along the  $\pi$ -conjugated structure of the monomer. The positions of the absorbance bands were weakly influenced by the structure of these monomers (see Diagram 2), including factors such as the size of the monomer and, above all, the presence of acceptor and donor electrons units. Since the main difference between monomers is the radical present in each molecule, the important point to consider is the presence of spectrum peaks corresponding to the electronic transitions derived from the new substituents on the bottom ring. In several cases, there are fine and hyperfine structures arising from interactions between both substituents; these interactions lead to expected, though complex, structures in the spectra [35]. In a different context, the known electronic transitions are shown in Fig. 4b; their presence helps to confirm the structure of the synthesized substances. The presence of a nitro group ( $-\text{NO}_2$ ) and its position in the aromatic ring seem to be the cause of the additional features of the spectrum. In monomer 4, where there are two nitro groups in the *ortho* and *para* positions, the absorbance peaks are sharpest, followed by monomer 5, in which there is a nitro group in the *ortho* position and a  $-\text{CF}_3$  substituent in the *para* position. The nitro substituent  $-\text{NO}_2$  is a deactivating group, i.e., is an electron attractor group; it is also a *meta* director. Due to this inductive effect, molecular stabilization is achieved by resonance. Groups such as  $-\text{CF}_3$ , are a special case, as they are deactivating groups and *ortho-para* directors because of the same inductive effect. In these groups, two unpaired electrons coming from the intrinsic negative charge are donated to the aromatic ring. The

electrons, however, are attracted to the same substituent due to the electronegativity of the group.

From the UV–Vis spectra, it is noticed that monomer 1 has two nitro groups which are *meta* directors, both groups in *meta* positions and attracting electronic density. This causes an inductive effect directed towards the same nitro groups, leading to dipole formation. Therefore, electronic transitions are represented in the UV–Vis spectrum by a very wide absorption band. Monomer 2 has a *meta* director, electro-attractor group ( $-\text{NO}_2$ ), and an *ortho-para* director, electro-attractor group ( $-\text{CF}_3$ ). Since both groups are deactivating, they have the same effect that the groups in monomer 1; electronic density is attracted by these groups, generating an inductive effect directed towards themselves and favoring dipole formation. Electronic transitions in the UV–Vis spectrum are characterized by a slightly narrower absorption band than that in monomer 1, due to a substituent change. Monomer 3 has a *meta* director, electro-attractor group ( $-\text{NO}_2$ ) and an *ortho-para* director, electro-attractor group ( $-\text{CF}_3$ ), both of which are deactivating groups. In this case, as in the previous ones, both substituents attract electronic density; however, because of the position of the  $-\text{NO}_2$  (*ortho*) substituent, dipole formation is weaker. The presence of this pair of substituent groups, and particularly their relative positions (*ortho* and *para*), also allows for a wide absorption band in the UV–Vis spectrum. Monomer 4 has two nitro substituent groups, both of them *meta* directors and electro-attractors. Both groups tend to attract electronic density because of their positions (*ortho* and *para*), although dipole formation is not as strong as in the previous case. Nevertheless, the presence of a nitro group in the *para* position gives a higher definition to the absorption band of the UV–Vis spectrum. In monomer 5 both groups are deactivating and attractors of electronic density. In this case, the nitro group is in *para* position and the  $-\text{CF}_3$  group is in *ortho* position, so that dipole formation occurs in the same way as in the previous case, though not as intense as in monomers 1 and 2; the presence of the nitro group in the *para* position contributes to the additional features found in the absorption band of the UV–Vis spectrum, as occurs in monomer 4. In monomer 6, both substituents are halogens, which are electro-attractors, so both attract electronic density that leads to dipole formation, though not as strong as in monomer 1. The lack of the nitro group makes the absorption band in the UV–Vis spectrum narrower than in those cases where there is at least one nitro substituent. For monomer 7, there is only a deactivating substituent ( $-\text{CF}_3$ ) in *para* position, which attracts electronic density and promotes an inductive effect leading to dipole formation; however, since there is only one substituent, the inductive effect is less noticeable than in the previous cases. As was the case for monomer 6, there is no nitro group in monomer 7, so the absorption band in the UV–Vis spectrum is narrow. Finally, monomer 8 has only one electro-attractor substituent ( $-\text{F}$ ) in *para* position, which attracts electronic density; nevertheless, the effect is even less noticeable than in the previous cases. This monomer does not have nitro groups or  $-\text{CF}_3$ , so the absorption band of the UV–Vis spectrum is wide.

The band gap is a fundamental parameter to establish the semiconducting character of these materials. It refers to the energy required by charge carriers to jump between the HOMO and the LUMO. Charge carrier mobility in monomers can be explained in terms of a hopping mechanism, according to which, charge carriers jump between adjacent molecules [36,37]. Unlike copolymers, monomers have only one type of molecule and their hopping process can be described in terms of an electronic exchange taking place through direct or indirect transitions. Direct transitions are typical for semiconductors with ordered structure, while indirect transitions take place in amorphous semiconductors [11–14]. The E-k diagrams of a semiconductor with direct band gap and another

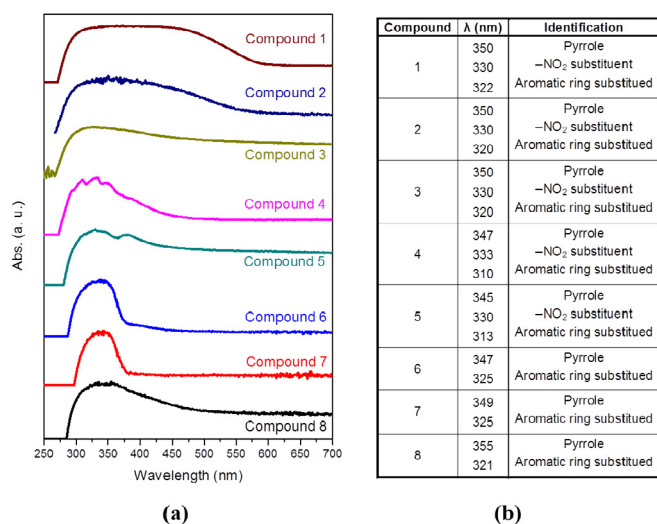


Fig. 4. (a) UV–Vis spectra of monomers and (b) characteristic UV–Vis absorptions in monomers.

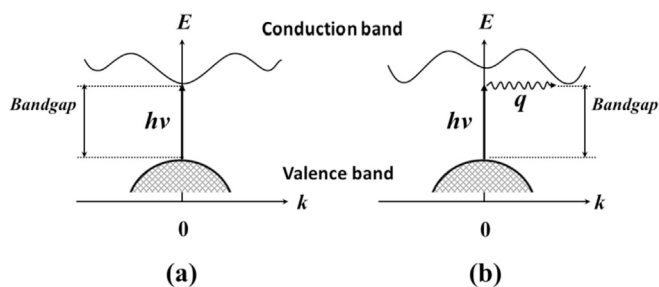


Fig. 5. (a) Direct band gap and (b) indirect band gap.

with indirect band gap, can be observed in Fig. 5a/b. The distinction concerns the relative positions of the minimum of the conduction band and the maximum of the valence band. In a direct band gap material, both positions occur at the same value of  $k$  ( $k=0$  in Fig. 5a). In an indirect band gap material, the minimum of the conduction band does not occur at the same position as the maximum of the valence band, but at another  $k$  value. In a direct band gap (see Fig. 5a) the electron wave vector does not change significantly during the photon absorption process. For the indirect band gap in Fig. 5b, the electron wave vector must change significantly for a transition from the valence band to the bottom of

conduction band to occur. It is not possible to perform this jump only by absorption of a photon: the transition must involve a phonon for momentum conservation [38]. Thus, it is worth determining whether the synthesized monomers have a crystalline structure permitting direct transitions. For this, DRX analysis of the monomers was performed and the results are shown in Fig. 6. The X-ray diffraction patterns of the monomers present well defined diffraction peaks, indicating polycrystalline samples and the likelihood of direct-type electronic transitions.

The direct band gap was determined first from the Tauc model, which assumes that the variation in the absorption coefficient ( $\alpha$ ) depends on the photon energy ( $h\nu$ ) [11,14]. The absorption coefficient ( $\alpha$ ) is thus given by:

$$\alpha = \ln\left(\frac{I}{d}\right)$$

In the above expression,  $T$  is the transmittance and  $d$  is the film's thickness. The photon energy is obtained through:

$$h\nu[\text{eV}] = \frac{hc}{\lambda}$$

where  $\lambda$  is the wavelength,  $h$  is Planck's constant and  $c$  is the speed of light. From these expressions, a plot of the absorption coefficient vs photon energy can be made, the absorption coefficient being  $(\alpha h\nu)^n$ , with  $n=2$  for direct transitions. Fig. 7 shows the resulting graph, in which the linear zone is identified, a tangent line is drawn and the intersection point with the  $h\nu$  axis is obtained. This point corresponds to the direct band gap. The numerical results are given

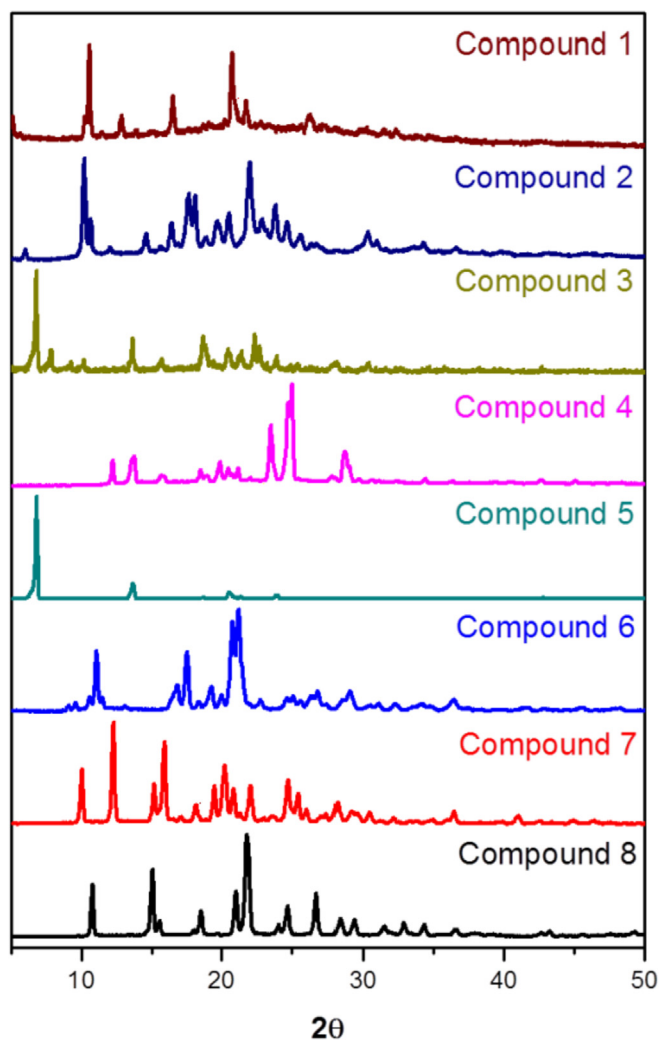


Fig. 6. DRX spectrum for monomers.

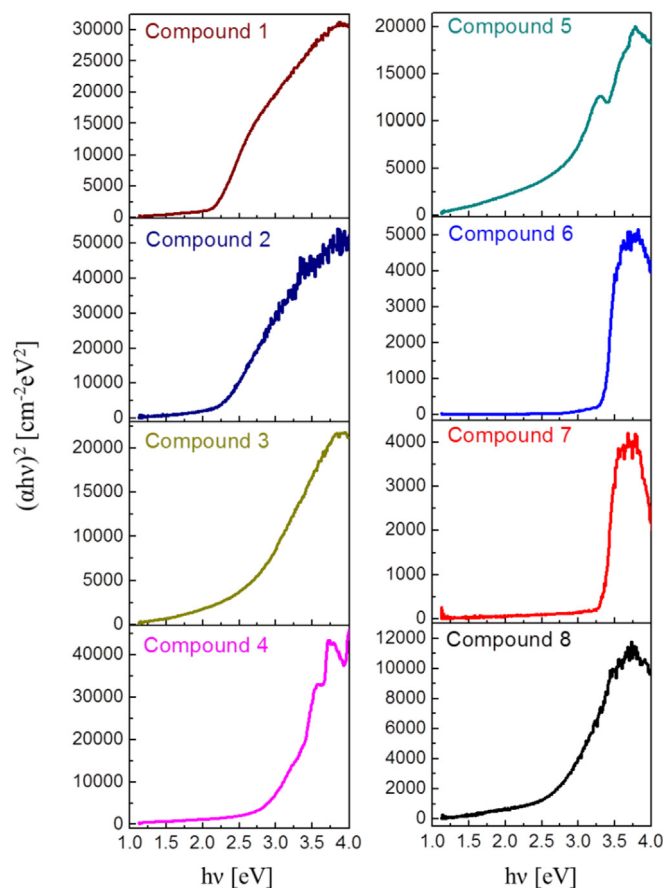
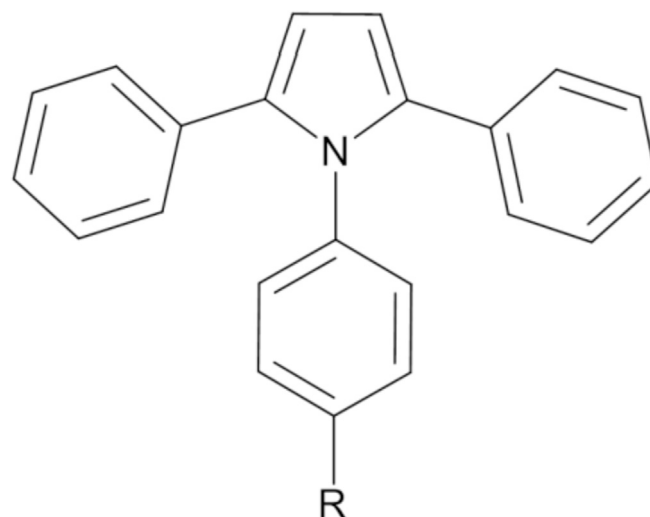


Fig. 7. Tauc plots for the determination of the direct band gap.

in Table 1 and show that monomers **6**, **7** and **8** have a band gap considerably different from that estimated by DFT calculation. It is worth noting that the Tauc band gap for monomer **8** has a value of 2.7 eV, within the range established for organic semiconductors [33], though much smaller than the theoretical value (4.5 eV). The difference may be due to a hopping-based charge transport process, in which electrical charges are easily displaced between ordered monomers.

In order to (i) corroborate the band gap obtained through Tauc method and (ii) determine the influence of thickness in the monomers' band gap, another analysis based on the Cody model was performed. Cody et al. [12,14] hypothesize that the band gap associated with the monomers should be determined by extrapolating the linear trend observed in the spectral dependence of  $(\alpha/h\nu)^2$ , over a range of  $h\nu$  values (Fig. 8). The abscissa axis intercept of this linear extrapolation corresponds to the Cody band gap. The results obtained can be compared to the DFT calculations and Tauc band gap in Table 1. From these results it is observed that there are no significant differences between the Tauc and Cody band gaps. Notice that both the Tauc and the Cody band gaps for monomers containing  $-\text{NO}_2$  groups is similar to that calculated using DFT. In monomers with  $-\text{CF}_3$  and  $-\text{F}$  groups, the smaller values of the experimental band gaps with respect to the theoretical band gaps may be due, as stated earlier, to a polycrystalline structure facilitating charge transport via a hopping process. Finally, it is observed that both Tauc and Cody band gaps are in the interval established for organic semiconductors [9]. Thus, the synthesized monomers may be considered for use in the production of optoelectronic devices.



R: H, O-Me, OH, CN, COOH,  $\text{NO}_2$

Diagram 1. Pyrrole derivative with electron-withdrawing groups.

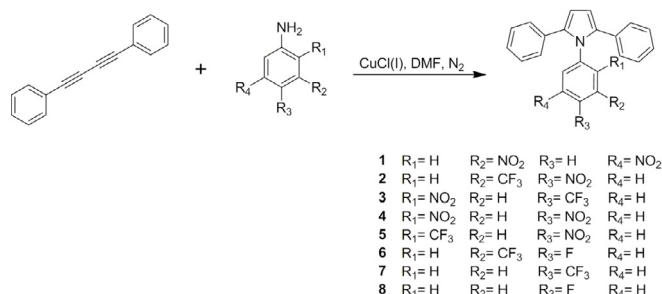


Diagram 2. Reactions of diacetylene with amines.

Monomers with  $-\text{NO}_2$  group should behave as *p* semiconductors and those having  $-\text{CF}_3$  and  $-\text{F}$  substituents as *n* semiconductors.

## 5. Conclusions

In this work, 8 new monomers containing pyrrole fragments with electron withdrawing groups have been processed according to the Reisch-Shulte procedure to synthesize the corresponding diphenyl-pyrrole derivatives. The HOMO energy values obtained for the synthesized monomers show relatively small variations, while the LUMO energy values change significantly. The differences may be related to the presence of substituents of differing nature in the skeleton of the monomers, which is a differentiating parameter in their charge-carrying properties. Based on the HOMO and LUMO values, monomer **1** shows the most promising behavior for semiconductor applications. Electronic transitions in the monomers depend on the type of radicals in the molecule and its crystallinity as well as of the position of the HOMO and LUMO of their orbitals. The band gap calculated by DFT for direct transitions is similar to that obtained by the Tauc and Cody methods for those monomers presenting  $-\text{NO}_2$  in their structure. While for monomers with electron-attracting functional groups, such as  $-\text{F}$  or  $-\text{CF}_3$ , electronic transport is favored and the experimental band gaps are considerably different from those obtained by DFT, although they are in an

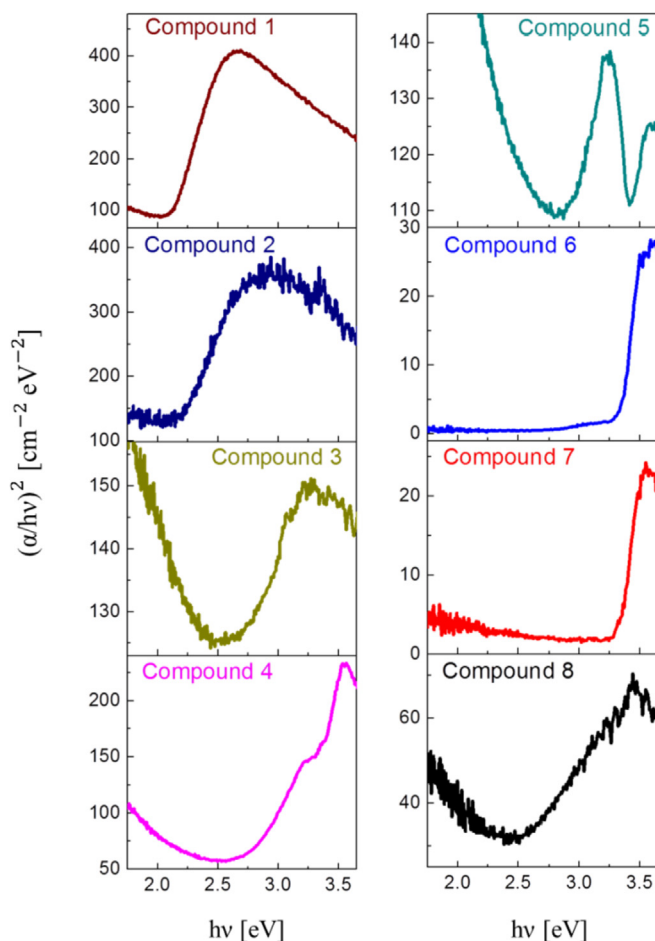


Fig. 8. Cody plot for the determination of the direct band gaps.



acceptable range for use in the manufacture of optoelectronic devices, such as OLEDs.

## Acknowledgments

The authors want to thank Adriana Tejada, María Teresa Vázquez, Oralia Jiménez, Alberto López, Gerardo Cedillo, Miguel A. Canseco and Alejandro Pompa for technical help. Many thanks are also due to DGAPA, UNAM for grants corresponding to the DGAPA PAPIIT IN203816 and RN203816 projects. Olivia Monroy thanks CONACYT for financial support. M.E. Sánchez-Vergara acknowledges financial support from Anahuac México University, project number NNAIASEVM16070616.

## References

- [1] B. Geffroy, P. Roy, C. Prat, Organic light-emitting diode (OLED) technology: materials, devices and display technologies, *Polym. Int.* 55 (2006) 572–582.
- [2] H. Sirringhaus, 25th anniversary article: organic field-effect transistors: the path beyond amorphous silicon, *Adv. Mater.* 26 (2014) 1319–1335.
- [3] L. Torsi, M. Magliulo, K. Manoli, G. Palazzo, Organic field-effect transistor structures: a tutorial review, *Chem. Soc. Rev.* 42 (2013) 8612–8628.
- [4] Z. Yin, J. Wei, Q. Zheng, Interfacial materials for organic solar cells: recent advances and perspectives, *Adv. Sci.* 3 (2016) 1–37, 1500362.
- [5] A. Facchetti, Semiconductors for organic transistors, *Mater. Today* 10 (2007) 28–37.
- [6] M. Bendikov, F. Wudl, D.F. Perepichka, Tetrathiafulvalenes, oligoacenes, and their buckminsterfullerene derivatives: the brick and mortar of organic electronics, *Chem. Rev.* 104 (2004) 4891–4946.
- [7] H. Ullah, S. Bibi, A.A. Tahir, T.K. Mallick, Density functional theory study of selenium-substituted low-bandgap Donor–Acceptor–Donor polymer, *J. Phys. Chem. C* 120 (2016) 27200–27211.
- [8] R. Salcedo, Aromaticity and electronic properties of heterosuperbenzene (heterohexabenzocoronene), *J. Mol. Model.* 13 (2007) 1027–1031.
- [9] W.R. Salaneck, R.H. Friend, J.L. Brédas, Electronic structure of conjugated polymers: consequences of electron–lattice coupling, *Phys. Rep.* 319 (1999) 231–251.
- [10] A.M. Teale, F. De Proft, D.J. Tozer, Orbital energies and negative electron affinities from density functional theory: insight from the integer discontinuity, *J. Chem. Phys.* 129 (2008) 1–12, 44110.
- [11] J. Tauc, Optical properties and electronic structure of amorphous Ge and Si, *Mater. Res. Bull.* 3 (1968) 37–46.
- [12] G.D. Cody, B.G. Brooks, B. Abeles, Optical absorption above the optical gap of amorphous silicon hydride, *Sol. Energy Mater.* 8 (1982) 231–240.
- [13] N. Laidani, R. Bartali, G. Gottardi, M. Anderle, P. Cheyssac, Optical absorption parameters of amorphous carbon films from forouhi–bloomer and tauc–lorentz models: a comparative study, *J. Phys. Condens. Matter* 20 (2008) 1–8, 015216.
- [14] T.M. Mok, S.K. O’Leary, The dependence of the Tauc and Cody optical gaps associated with hydrogenated amorphous silicon on the film thickness:  $\alpha$  Experimental limitations and the impact of curvature in the Tauc and Cody plots, *J. Appl. Phys.* 102 (2007) 1–9, 113525.
- [15] Y. Liu, J. Zhang, Y. Liu, G. Yu, Z. Ge, Structure-property relationships based on Phenyl-1 H - pyrrole end-capped thiophene semiconductors, *Aust. J. Chem.* 65 (2012) 1252–1256.
- [16] V. Bhardwaj, D. Gumber, V. Abbot, S. Dhiman, P. Sharma, Pyrrole: a resourceful small molecule in key medicinal hetero-aromatics, *RSC Adv.* 5 (2015) 15233–15266.
- [17] Y. Qiao, J. Zhang, W. Xu, D. Zhu, Incorporation of pyrrole to oligothiophene-based quinoids endcapped with dicyanomethylene: a new class of solution processable n-channel organic semiconductors for air-stable organic field-effect transistors, *J. Mater. Chem.* 22 (2012) 5706–5714.
- [18] B.L. Reid, S.B. Briggs, L.E. Karagiannidis, S. Muzzioli, P. Raiteri, M.E. Light, S. Stagni, P. Brulatti, P.A. Gale, M.I. Ogden, M. Massi, Blue emitting C<sub>2</sub>-symmetrical dibenzothiazolyl substituted pyrrole, furan and thiophene, *J. Mater. Chem. C* 1 (2013) 2209–2216.
- [19] G. Huerta, L. Fomina, L. Rumsh, M.G. Zolotukhin, New polymers with N-phenyl pyrrole fragments obtained by chemical modifications of diacetylene containing-polymers, *Polym. Bull.* 57 (2006) 433–443.
- [20] J. Godínez Sánchez, L. Fomina, L. Rumsh, Novel hyperbranched molecules containing pyrrole units from diacetylene compounds, *Polym. Bull.* 64 (2009) 761–770.
- [21] L. Fomina, G.Z. Galán, M. Bizarro, J.G. Sánchez, I.P. Zaragoza, R. Salcedo, Semiconductor behavior of 2,5-aromatic disubstituted pyrroles, viewed from an experimental and theoretical perspective, *Mater. Chem. Phys.* 124 (2010) 257–263.
- [22] L. Fomina, J.G. Sánchez, J.A. Olivares, F.L.S. Cuppo, L.E. Sansores, R. Salcedo, Electronic properties of hyperbranched compounds derived by pyrrole, *J. Mol. Struct.* 1074 (2014) 534–541.
- [23] L. Fomina, C. León, M. Bizarro, A. Baeza, V. Gómez-Vidales, L.E. Sansores, R. Salcedo, TTF derivative of 2,5-aromatic disubstituted pyrrole, synthesis and electronic study, *J. Mol. Struct.* 1108 (2016) 370–377.
- [24] J. Reisch, K.E. Schulte, Pyrrol-Derivate aus Diacetylenen, *Angew. Chem.* 73 (1961), 241–241.
- [25] K.E. Schulte, J. Reisch, H. Walker, Dipyrrole und Porphin aus Acetylenverbindungen, *Arch. Pharm* 299 (1966) 1–7.
- [26] K.E. Schulte, J. Reisch, H. Walker, Eine neue Pyrrolsynthese aus Butadiin-Derivaten, *Chem. Ber.* 98 (1965) 98–103.
- [27] M.J. Frisch, G.W. Trucks, H.B. Schlegel, G.E. Scuseria, M.A. Robb, J.R. Cheeseman, G. Scalmani, V. Barone, B. Mennucci, G.A. Petersson, H. Nakatsuji, M. Caricato, X. Li, H.P. Hratchian, A.F. Izmaylov, J. Bloino, G. Zheng, J.L. Sonnenberg, M. Hada, M. Ehara, K. Toyota, R. Fukuda, J. Hasegawa, M. Ishida, T. Nakajima, Y. Honda, O. Kitao, H. Nakai, T. Vreven, J.A. Montgomery Jr., J.E. Peralta, F. Ogliaro, M. Bearpark, J.J. Heyd, E. Brothers, K.N. Kudin, V.N. Staroverov, R. Kobayashi, J. Normand, K. Raghavachari, A. Rendell, J.C. Burant, S.S. Iyengar, J. Tomasi, M. Cossi, N. Rega, N.J. Millam, M. Klene, J.E. Knox, J.B. Cross, V. Bakken, C. Adamo, J. Jaramillo, R. Gomperts, R.E. Stratmann, O. Yazyev, A.J. Austin, R. Cammi, C. Pomelli, J.W. Ochterski, R.L. Martin, K. Morokuma, V.G. Zakrzewski, G.A. Voth, P. Salvador, J.J. Dannenberg, S. Dapprich, A.D. Daniels, Ö. Farkas, J.B. Foresman, J.V. Ortiz, J. Cioslowski, D.J. Fox, Gaussian 09, Revision A.1, Gaussian, Inc., Wallingford, CT, 2009.
- [28] A.D. Becke, Density-functional exchange-energy approximation with correct asymptotic behavior, *Phys. Rev. B* 38 (1988) 3098–3100.
- [29] J.P. Perdew, Y. Wang, Accurate and simple analytic representation of the electron-gas correlation energy, *Phys. Rev. B* 45 (1992) 13244–13249.
- [30] A.S. Hay, Oxidative coupling of acetylenes. II, *J. Org. Chem.* 27 (1962) 3320–3321.
- [31] J. Roncali, Molecular engineering of the band gap of p -conjugated systems: facing technological applications, *Macromol. Rapid Commun.* 28 (2007) 1761.
- [32] N.S. Tuzun, F. Bayata, A.S. Sarac, An experimental and quantum mechanical study on electrochemical properties of N-substituted pyrroles, *J. Mol. Struct. THEOCHEM* 857 (2008) 95–104.
- [33] G. García Moreno, Organic Semiconductors Pi-conjugated Based on Tiofenos. A Theoretical Study, Doctoral Thesis, Universidad de Jaén, 2012, 978-84-8439-683-3.
- [34] N. Laidani, R. Bartali, G. Gottardi, M. Anderle, P. Cheyssac, Optical absorption parameters of amorphous carbon films from Forouhi–Bloomer and Tauc–Lorentz models: a comparative study, *J. Phys. Condens. Matter* 20 (2008) 1–8, 15216.
- [35] B.C. Chang, D. Yu, D. Cullin, B. Rehfuss, J. Williamson, W.M. Fawzy, X. Zheng, S. Fei, M. Heaven, Rotational, fine and hyperfine structure in the high resolution electronic spectrum of ArOH and ArOD, *J. Chem. Phys.* 95 (1991) 7086–7098.
- [36] M. Pope, C.E. Swenberg, *Electronic Processes in Organic Crystals and Polymers*, second ed., Oxford, New York, 1999.
- [37] G. Hadziioannou, G.G. Malliaras, *Semiconducting Polymers*, Wiley-VCH, Weinheim, 2007.
- [38] M. Fox, *Optical Properties of Solids*, first ed., Oxford University Press, USA, 2001.